A Short Review of Microwave and Laser Discharges for Supersonic Flow Control

D. Knight

D. Knight
(Rutgers, The State University of New Jersey)

E-mail: doyleknight@gmx.com

DOI : 10.12762/2015.AL10-02

A Short Review of Microwave and Laser Discharges for Supersonic Flow Control

Energy deposition by electromagnetic discharge (*e.g.*, arc, laser, microwave) is an emerging field of research in flow and flight control. Major advantages of this approach include fast response time, capability for customization of discharge, and off-body modification of the flow. Recent computational and experimental research in energy deposition are described and future needs identified.

Introduction

Energy deposition by pulsed laser and microwave discharge has received significant interest in the past several decades as a promising technique for flow control at high speeds. In this article we present a brief review of selected experimental and theoretical studiess to illustrate the potential of this emerging technology. Additional information may be obtained from several recent reviews including Zheltovodov [30], Fomin *et al.* [7], and Knight [12].

Microwave Discharge

Introduction

The phenomenon of pulsed microwave discharge (breakdown) in air is characterized by a bright flash of light and formation of a complex plasma structure depending on the microwave frequency (wavelength) and ambient pressure. An example of the variety of plasma shapes is presented in figure 1 from Kolesnichenko [13]. The Paschen curve (MacDonald [19], Fridman and Kennedy [8]) defines the breakdown electric field strength E as a function of the product of the ambient pressure p and microwave wavelength λ. An extensive literature on microwave discharge is available; for example, see Lebedev [17, 18].

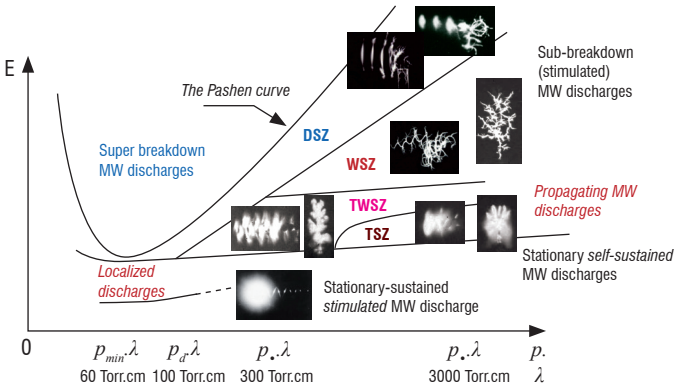

Figure 1 – Types of microwave discharges [13]. DSZ: discharge with straight channels, WSZ: discharge with curved channels, TWSZ, TSZ: variant of WSZ

We summarize the results of three experiments on the interaction of a microwave discharge with a test model in supersonic flow. The flow conditions are summarized in table 1. Kolesnichenko *et al.* [15] and Lashkov *et al.* [16] performed experiments at St. Petersburg State University, Russian Federation. Exton *et al.* [6] conducted experiments at NASA Langley Research Center, Hampton, Virginia.

Quantity	K2001	E2001	L2004
Mach number	*1.7*	*6.0*	*2.1*
Stagnation pressure (kPa)	*39.5*	*631*	*30.5*
Stagnation temperature (K)	*316*	*574*	*300*
MW frequency (GHz)	*9*	*16*	*9*
MW peak power (kW)	*210*	*425*	*210*
MW pulse (μs)	*1.2 - 2.2*	*3.5*	*1.2*

Table 1 – K2001: Kolesnichenko *et al.* [15]. E2001: Exton *et al.* [6]. L2004: Lashkov *et al.* [16]

Kolesnichenko et al. 2001

Kolesnichenko *et al.* [15] conducted a series of experiments to examine the interaction of a microwave-generated plasma on the drag of a blunt cylinder at Mach 1.7 at a freestream static pressure p_∞=8 kPa and static temperature T_∞=200 K. The microwave pulse was generated by a klystron operating at 9 GHz with peak power of 210 kW and pulse duration τ=1.2 to 2.2 μs. The estimated reduced field E/N (where E is the magnitude of the electric field and N is the particle concentration) is 80 to 100 Townsend. The discharge generated multiple plasmoids (up to three) upstream of the blunt cylinder which convected downstream at approximately the freestream velocity. The plasmoids were initially formed on the centerline of the cylinder upstream of the blunt body shock.

Schlieren images of the interaction are shown in figures 2(a) and 2(b) where the flow is from right to left. The blunt body shock generated by the blunt cylinder is visible. At $t=21\,\mu s$ the plasmoid has reached the blunt body shock causing a lensing forward (*i.e.*, upstream) of the shock. The experimental surface pressure on the cylinder face at the centerline *vs* time is shown in figures 3(a) and 3(b) for air and CO_2, respectively, for models of differing diameter. In all cases a dramatic reduction in surface pressure is observed resulting in a momentary reduction in drag.

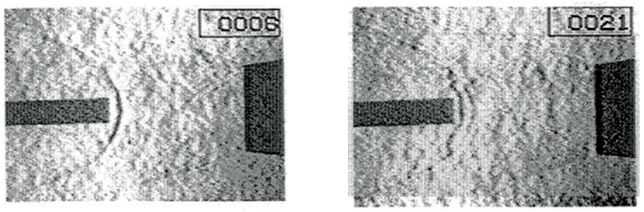

(a) $t=6\,\mu s$ (b) $t=21\,\mu s$

Figure 2 – Schlieren images of microwave discharge [15]

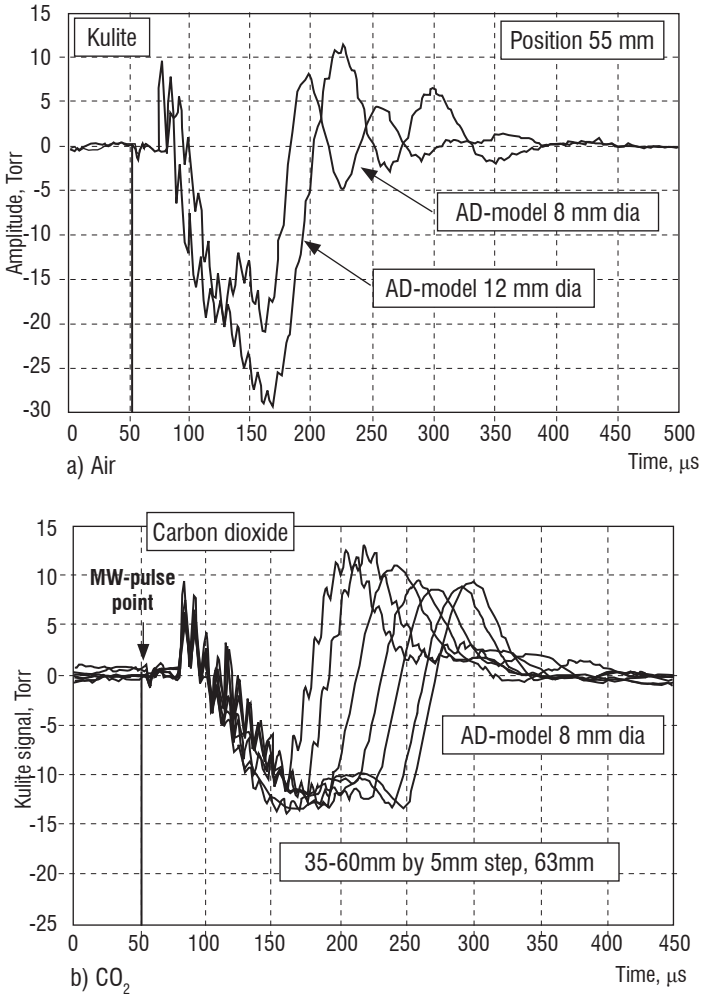

Figure 3 – Surface pressure *vs* time for microwave discharge (AD means "aerodynamic") [15]

Exton 2001

Exton *et al.* [6] conducted an experiment to examine the interaction of a microwave-generated plasma with a blunt cylinder at Mach 6 at a freestream static pressure $p_\infty=0.4$ kPa and static temperature $T_\infty=70$ K. The microwave pulse was generated by a Ku-band klystron (15.8 – 17.3 GHz) with a peak power of 425 kW and pulse duration $\tau\leq3.5\,\mu s$. A 10-mCi ^{90}Sr radioactive source emitting 0.54 MeV electrons was used as an initiator for the discharge. The experimental configuration is shown in figure 4. The duty cycle was 0.001 implying no interaction between individual pulses. Figure 5 displays a time-averaged Schlieren image. The microwave discharge is focused just upstream of the shock wave, and has no apparent effect on the shock standoff distance. The plasma becomes reflective to microwave radiation during the early stages of the microwave pulse due to the increase in the electron concentration, thereby creating an effective plasma mirror.

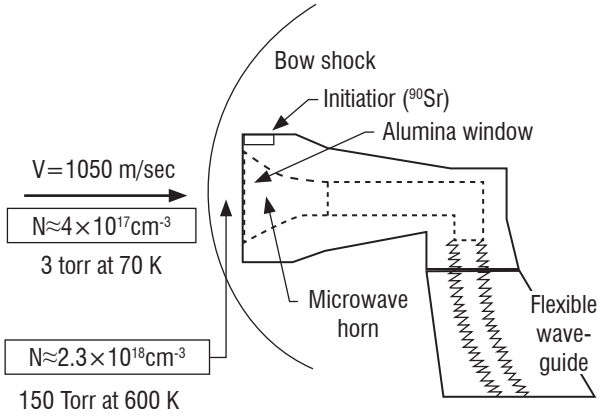

Figure 4 – Experimental configuration for microwave discharge [6]

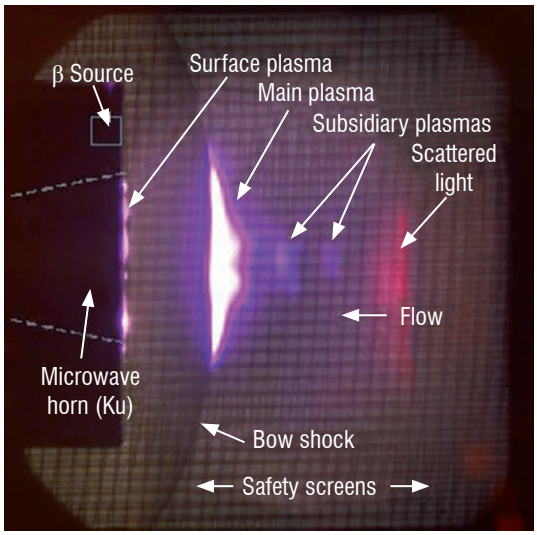

Precursor Plasma at Mach 6

Figure 5 – Schlieren image for microwave discharge [6]

Lashkov *et al.* 2004

Lashkov *et al.* (2004)[16] conducted experiments to evaluate the interaction of a microwave discharge on blunt and hemisphere cylinders at Mach 2.1 in air at a freestream static pressure $p_\infty=3.3$ kPa and static temperature $T_\infty=159$ K. The microwave generator described in Kolesnichenko *et al.* [15] was used. The plasmoids were similarly formed initially on the centerline of the cylinder upstream of the blunt body shock.

Schlieren images for the interaction of the microwave-generated plasma with the blunt cylinder are presented in figure 6 for $t=20\,\mu s$ to 140 μs. The lensing forward of the shock seen in figures 6(c) to 6(f). The shock standoff distance at the centerline increases to nearly twice the undisturbed distance. The experimental pressure on the cylinder centerline, shown in figure 8(a), decreases from 28.7 kPa prior to the interaction to 9.3 kPa at $t=150\,\mu s$ due to the interaction, resulting in a significant momentary reduction in pressure drag on the cylinder.

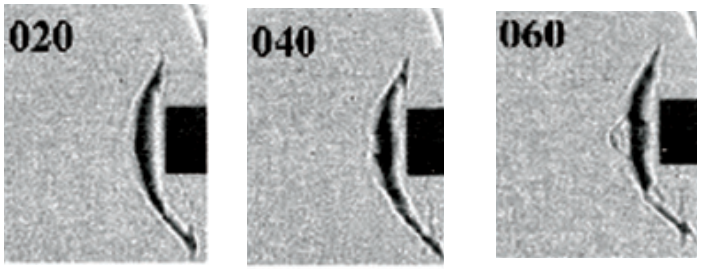

(a) t=20 μs (b) t=40 μs (c) t=60 μs

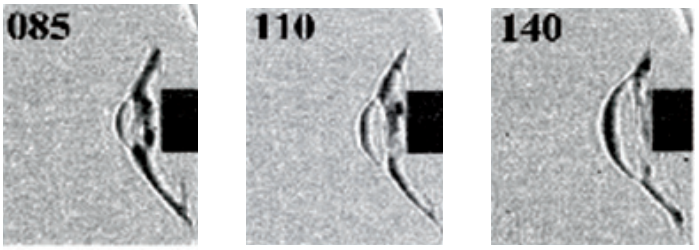

(d) t=85 μs (e) t=110 μs (f) t=140 μs

Figure 6 – Schlieren images for microwave discharge upstream of blunt cylinder [16]

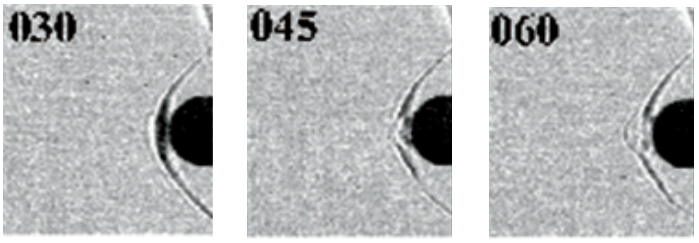

(a) t=30 μs (b) t=45 μs (c) t=60 μs

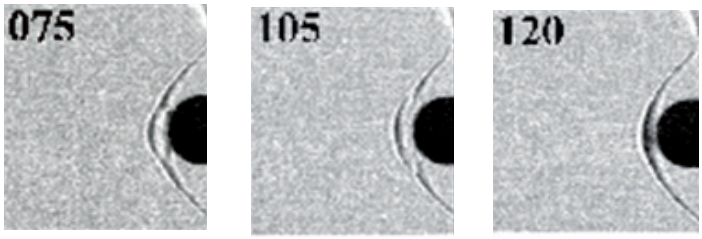

(d) t=75 μs (e) t=105 μs (f) t=120 μs

Figure 7 – Schlieren images microwave discharge upstream of hemisphere cylinder [16]

Schlieren images of the interaction of the microwave-generated plasma with the hemisphere cylinder are shown in figure 7. The interaction is similar to the blunt cylinder experiment of Kolesnichenko *et al.* [15]. The plasma causes the blunt body shock to lens forward beginning at t=60 μs. The centerline pressure (figure 8(b)) displays a similar dramatic decrease at t=100 μs due to the interaction of the plasma with the blunt body shock.

The effect of off-centerline initial location of the microwave-generated plasma was examined. Off-axis displacement up to D (where D is the cylinder diameter) were considered for the blunt cylinder. An impulse function was defined

$$I = \int_0^{t_f} \left(p_{CL}(t) - p_0(t) \right) A dt \qquad (1)$$

where $p_{CL}(t)$ is the time-dependent centerline pressure on the cylinder due to the interaction, p_o is the undisturbed centerline pressure, A is the cylinder frontal area and t_f is the duration of the interaction. It was observed that I<0 for displacements less than 0.15D (*i.e.*, drag reduction) and I>0 for displacements greater than 0.15D (*i.e.*, drag increase).

Laser Discharge

Introduction

The phenomenon of pulsed laser discharge (breakdown) was discovered in the 1960s [4, 20, 21, 22, 23]. The discharge is characterized by a bright flash of light at the focus of the laser beam and a sharp noise ("crack"). Three successive phases occur in the discharge which is typically tens of nanoseconds to microseconds in duration. The first phase is multi-photon ionization wherein multiple photons are absorbed by gas atoms resulting in ionization and release of electrons [10]. The second phase is inverse bremsstrahlung and cascade ionization wherein the free electrons gain energy by absorption of photons and ionize neutral particles leading to a cascade growth of free electrons and ions. The final phase is the formation of a plasma (ionization) wave due to the heating of the gas by the incident laser radiation and propagates towards the laser source [26].

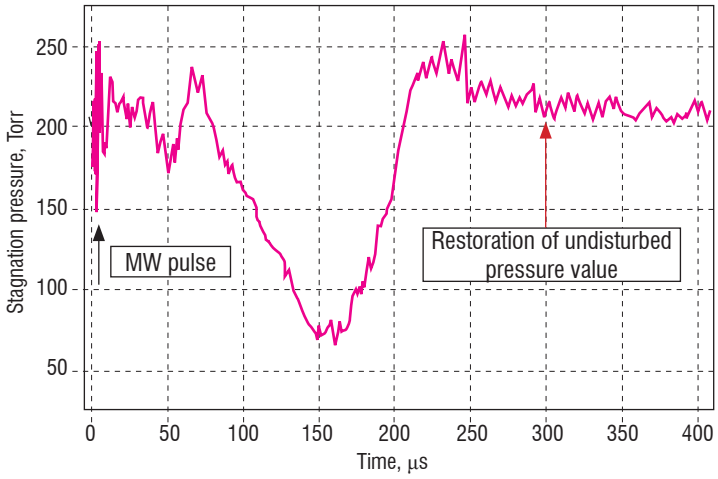

(a) Cylinder

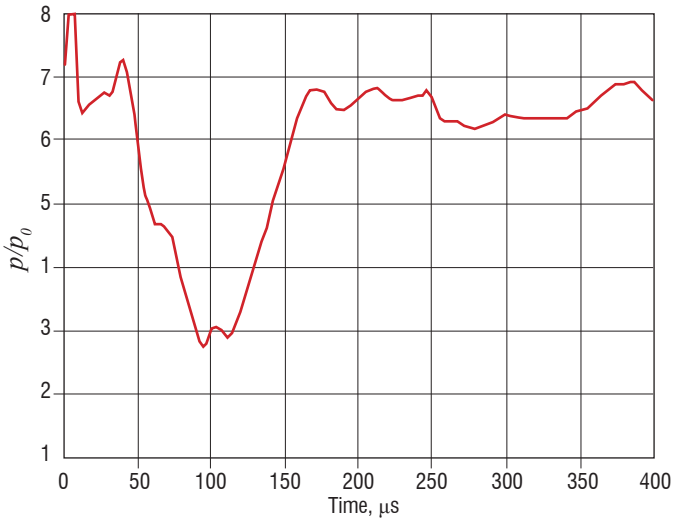

(b) Sphere

Figure 8 – p *vs* t on centerline of body for microwave discharge [16]

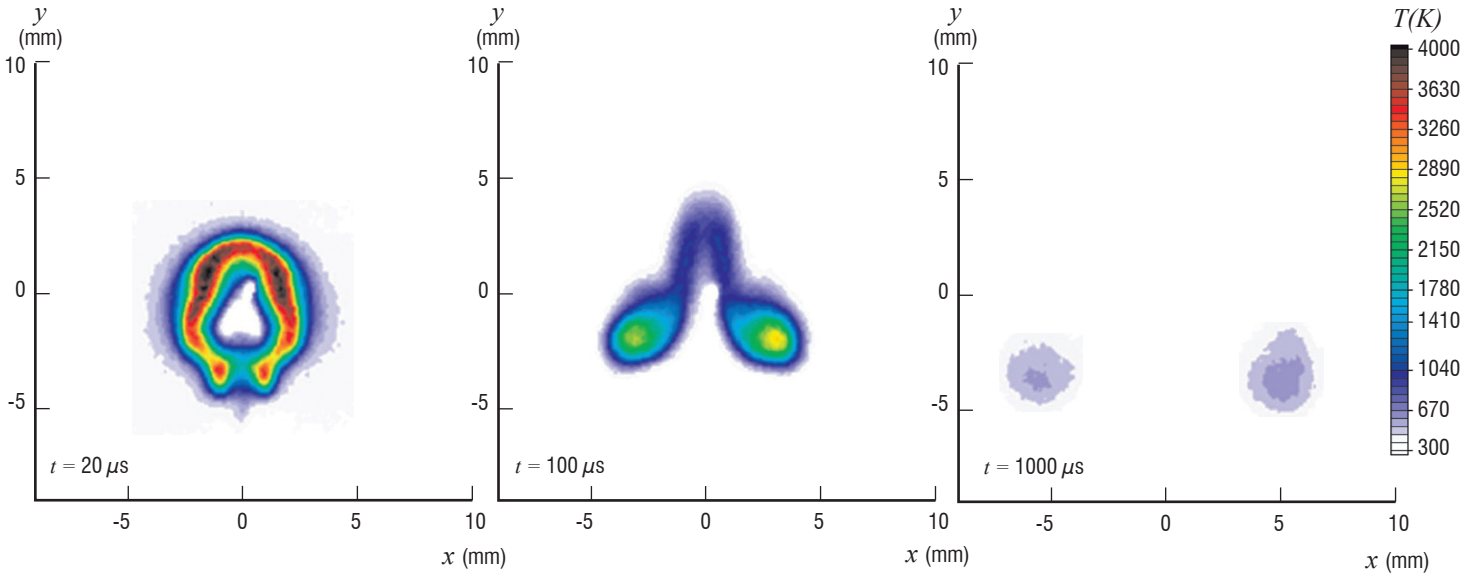

Figure 9 – T at t=20 μs to 1000 μs for laser discharge [9]

Subsequent to the discharge phase, a blast wave forms due to the high pressure and temperature generated by the laser discharge. The blast wave becomes spherical at distances large compared to the laser discharge focal volume and the pressure rise decreases with distance from the discharge. The plasma wave formed during the discharge generates a jet directed toward the laser source forming a toroidal vortex. The temperature in the plasma decreases in time due to mixing and radiation. Figure 9 from Glumac *et al.* [9] displays the measured temperature for a 150 mJ Nd:YAG (532 nm) discharge of 6.5 ns in air at ambient conditions. Detailed reviews of laser discharge in gases are presented in Raizer [27], Ostrovskaya and Zaidel [25] and Morgan [24].

We summarize the results of three experiments on the interaction of a laser discharge with a test model in supersonic flow. The flow conditions are summarized in table 2. Tretyakov *et al.* [29] performed experiments at the Khristianovich Institute of Theoretical and Applied Mechanics in Novisibirsk, Russian Federation. Adelgren *et al.* [1] conducted experiments at Rutgers, The State University of New Jersey. Schülein *et al.* [28] performed experiments at the German Aerospace Center DLR in Göttingen, Germany.

Quantity	T1996	A2005	S2010
Mach number	*2*	*3.45*	*2.0*
Stagnation pressure (kPa)	*450*	*1400*	*180*
Stagnation temperature (K)	*293*	*290*	*270*
Laser pulse frequency (kHz)	*12.5 to 100*	*n/a*	*n/a*
Laser pulse duration (ns)	*1200*	*10*	*5*
Body diameter (mm)	*6.0*	*25.4*	*60*

Table 2 – T1996: Tretyakov *et al.* [29]. A2005: Adelgren *et al.* [1]. S2010: Schülein *et al.* [28]

Tretyakov *et al.* 1996

Tretyakov *et al.* [29] measured the drag on a cone-cylinder and hemisphere-cylinder at M_∞=2 in argon using a high frequency CO_2 laser discharge upstream of the body. The experimental configuration is shown in figure 10 and the experimental conditions are indicated in table 2.

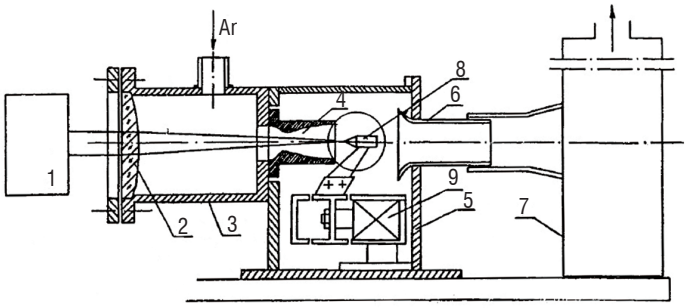

1– CO_2 laser 2– focusing lens 3– plenum chamber 4– nozzle unit 5– working chamber 6– diffuser 7– exhaust chamber 8– model 9– aerodynamic window

Figure 10 – Experimental configuration for laser discharge [29]

The distance l of the focal point of the laser discharge from the test model was varied between one and two diameters upstream on the centerline. The measured drag (figure 11) shows a substantial reduction up to 45%. The parameter L is the distance of the body from the nozzle exit. The effect of the location and frequency of the laser discharge can be understood by replotting the data in terms of the dimensionless pulse period

$$\tau = \frac{U_\infty}{fl} \qquad (2)$$

where f is the pulse repetition frequency, U_∞ is the freestream velocity and l is the distance of the laser focus to the test model. The parameter τ is the ratio of the elapsed time between pulses to the time required for the freestream flow to travel between the pulse location and the leading edge of the body. Results shown in figure 12 indicate that the maximum drag reduction is achieved at $\tau \approx 1$.

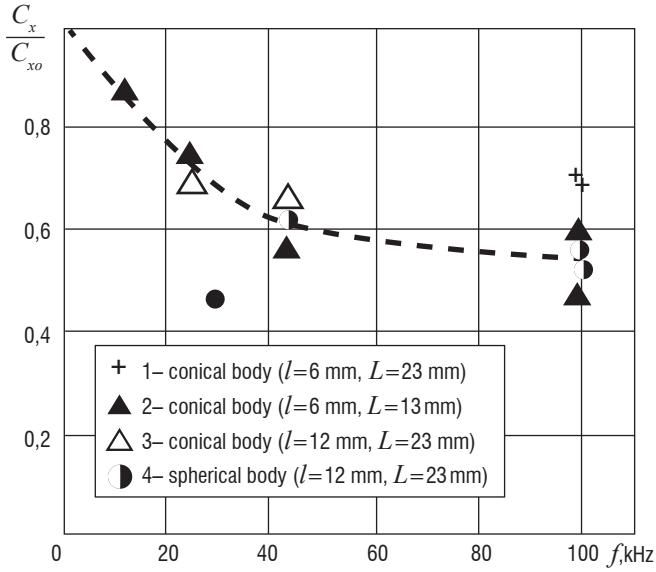

Figure 11 – Drag coefficient ratio *vs* frequency for laser discharge [29]

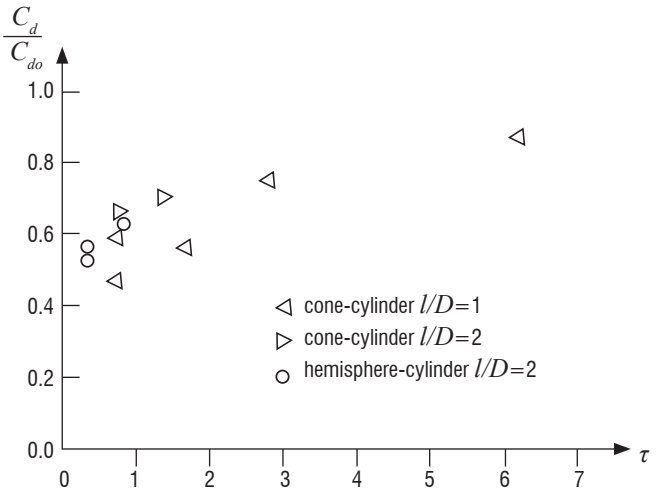

Figure 12 – Drag coefficient *vs* τ for laser discharge [29]

Adelgren *et al.* 2005

Adelgren *et al.* [1] investigated the interaction of a laser discharge in air with a sphere at Mach 3.45. The experimental configuration is illustrated in figure 13 and the experimental conditions are listed in table 2. An Nd:YAG (532 nm) laser was focused upstream of a hemisphere cylinder on the centerline. The focal volume is approximately 3.0 mm³. Discharge energies from 13 mJ to 283 mJ were considered. Experiments were performed with and without an impinging oblique shock wave (generated by the 15° compression ramp indicated in figure 13) intersecting the blunt body shock generated by the sphere.

Results for the interaction of a 283 mJ laser pulse with the sphere are shown in figure 14. The bright spot indicates the location of the laser discharge (figure 14(a)) and remains in all subsequent images due to saturation of the CCD camera. The blast wave generated by the discharge impacts the sphere at t=30 μs (figure 14(b)). The heated plasma intersects the blunt body shock causing it to lens upstream while a toroidal vortex forms (figure 14(c)). Eventually the plasma convects downstream and the flow returns to steady state (figure 14(d)).

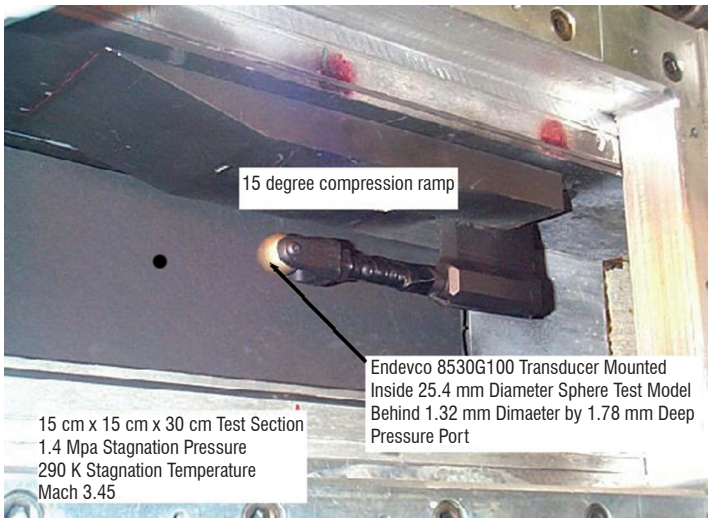

Figure 13 – Experimental configuration for laser discharge [1]

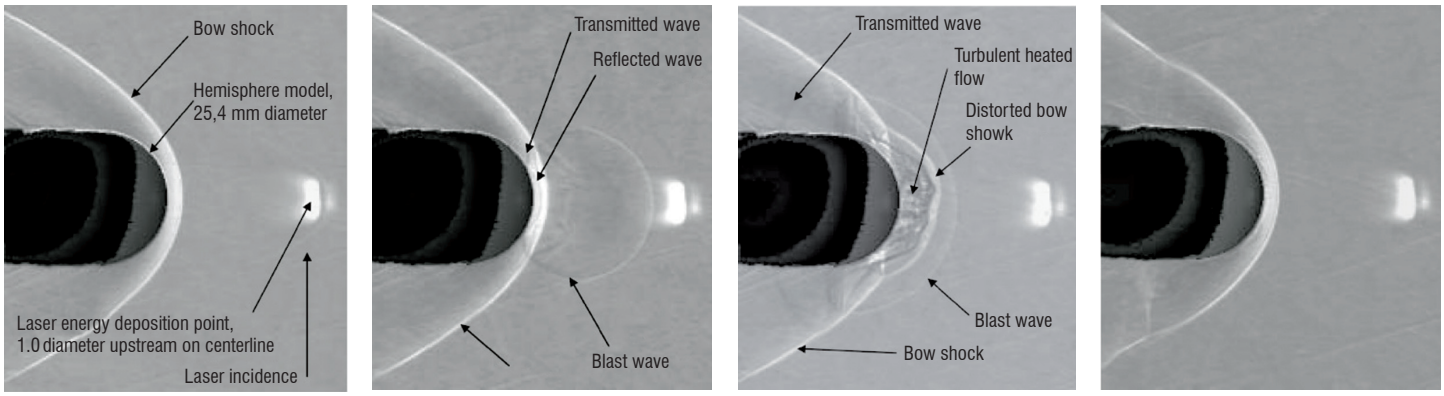

(a) t=0 μs (b) t=30 μs (c) t=60 μs (d) t=120 μs

Figure 14 – Schlieren images of interaction of laser discharge (283 mJ) with sphere [1]

Figure 15 displays the surface pressure on the forward face of the hemisphere vs time where the surface pressure is normalized by the stagnation pressure p_{O_2} on the sphere in the absence of the laser discharge. The impact of the blast wave on the sphere results in an initial pressure rise $\tau \approx 30$ μs followed by an sudden expansion. The interaction of the plasma with the blunt body shock generates a recompression and the pressure relaxes to its steady state distribution. The temporal history of the centerline pressure for three different energy pulses is shown in figure 16. The initial peak pressure associated with the impact of the blast on the sphere increases with laser discharge energy; however, the minimum pressure achieved during the expansion is insensitive to the laser discharge energy.

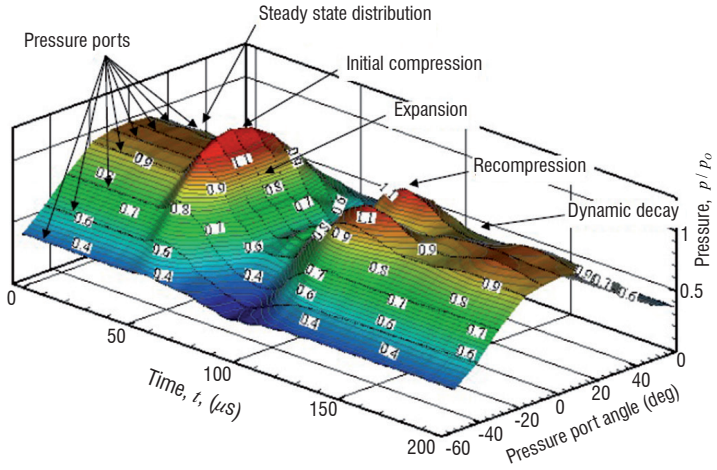

Figure 15 – p / p_O *vs* t on front surface for interaction of laser dischage with sphere [1]

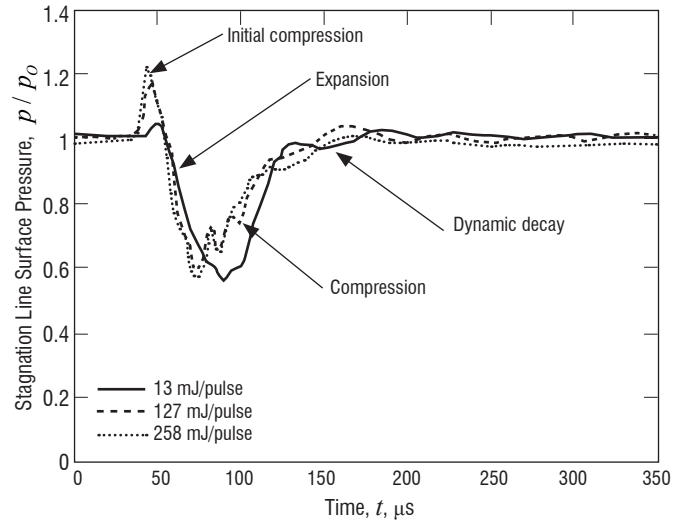

Figure 16 – Centerline pressure vs time for different laser pulse energy [1]

Schülein *et al.* 2010

Schülein *et al.* [28] performed an experimental investigation of the interaction of single- and double-pulsed laser discharge in air with a hemisphere cylinder at Mach 2. The experimental configuration is shown in figure 17 and the experimental conditions listed in table 2. An Nd:YAG (532 nm) laser was focused through the centerline of the hemisphere cylinder to a point upstream. The focal volume is approximately ellipsoidal with major axis of 1 mm and minor axes of 0.2 mm. Discharge energies from 151 mJ to 666 mJ were considered.

Experimental shadowgraphs for Q=333 mJ are shown in figure 18. Figure 18(a) indicates the heated region formed by the laser discharge, the blast wave which has rapidly assumed a spherical shape and the blunt body shock ahead of the hemisphere. The blast wave expands radially outwards from the initial location of the laser discharge. Figure 18(b) shows the instant of blast wave impact on the centerline. At instant earlier the blast wave intersected the blunt body shock and a transmitted shock propagated into the space between the blunt body shock and the hemisphere. Note that the plasma has not yet reached the blunt body shock. Figure 18(c) shows the instant of intersection of the plasma with the blunt body shock which lenses forward due to the lower Mach number of the heated region. Figure 18(d) displays the toroidal vortex formed by the Richtmyer-Meshkov instability associated with the intersection of the boundary of the heated region with the blunt body shock.

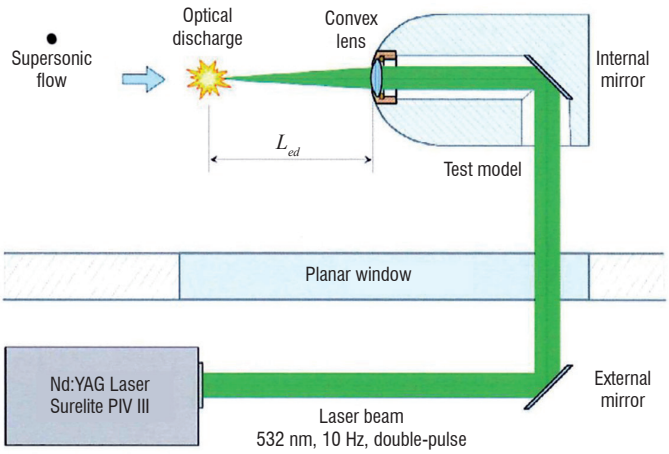

Figure 17 – Experimental configuration for laser discharge [28]

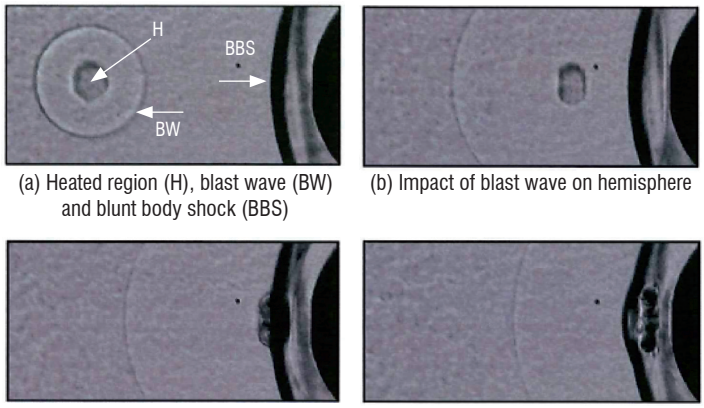

(a) Heated region (H), blast wave (BW) and blunt body shock (BBS)

(b) Impact of blast wave on hemisphere

(c) Intersection of heated region with blunt body shock

(d) Richtmeyer-Meshkov instability and formation of toroidal vortex

Figure 18 – Experimental shadowgraphs for single laser discharge Q=333 mJ [28]

Modeling

Introduction

The physical processes associated with pulsed laser or microwave discharge in air are complex, involving finite rate chemical reactions, real gas effects, radiation and plasma dynamics. A complete description of these phenomena is therefore difficult, and therefore modeling of such pulsed discharges is typically simplified based upon a variety of assumptions. We present three selected examples of models. Kandala and Candler [11] developed a realistic model of laser discharge and applied the model to the simulation of the interaction of the discharge plasma with a hemisphere and an Edney IV interaction. Azarova *et al.* [3] and Anderson and Knight [2] applied a simpler perfect gas model to the interaction of a microwave discharge with a blunt cylinder.

Kandala and Candler

Kandala and Candler [11] simulated the interaction of a laser discharge with a sphere and an Edney IV interaction (Edney [5]) corresponding to the experiments of Adelgren *et al.* [1]. The laser discharge model assumes the existence of a small concentration of electrons (*i.e.*, assumes multi-photon ionization has occurred) and approximates the inverse-bremsstrahlung absorption by absorptivity coefficient κ_a. The intensity I of the laser radiation in the beam direction x is

$$\frac{dI}{dx} = -\kappa_a I \tag{3}$$

The absorption coefficient is

$$\kappa_a = \Sigma N_e \left(1 - e^{-hc/\lambda kT_e}\right) \tag{4}$$

where Σ is the characteristic interaction cross-sectional area, N_e is the electron concentration, h is Planck's constant, c is the speed of light, λ is the laser wavelength, k is Boltzmann's constant and T_e is the electron temperature. Since the laser-generated plasma becomes opaque to the radiation with increase in the electron concentration, a reflectivity coefficient is implemented

$$\kappa_r = A\left(\log Z + B\right) \tag{5}$$

where $0<\kappa_r<1$ and Z is the degree of ionization. The values of Σ, A and B are determined by comparison of the computed and experimental blast wave for the laser discharge in ambient air. The laser radiation model was coupled with an eleven species model for air (N_2, O_2, NO, N, O, $N^{+,2}$, $O^{+,2}$, NO^+, N^+, O^+ and electrons). The governing equations include the conservation of mass for each specie and mass-averaged momentum, and conservation of vibrational, electronic and total energy.

Kandala and Candler simulated a 160 mJ Nd:YAG laser discharge and its interaction with a sphere at Mach 3.45 corresponding to the experiment of Adelgren *et al.* [1]. The laser discharge was focused upstream of the sphere on the centerline. Figure 19 displays the computed surface pressure and heat transfer on the centerline vs time where p_o and q_o are the centerline pressure and heat transfer in the undisturbed flow. The initial increase in pressure and heat transfer at $t=25\,\mu$s corresponds to the impact of the blast wave on the sphere. The subsequent reduction in both pressure and heat transfer is due to the interaction of the plasma with the blunt body shock resulting in a lensing forward of the shock and expansion wave impacting the sphere. As the plasma convects towards the sphere the surface pressure increases; however, a significant spike in heat transfer is noted.

Kandala and Candler performed several simulations of a laser discharge and its interaction with an Edney IV flowfield at Mach 3.45 corresponding to the experimental configuration of Adelgren *et al.* [1]. Different focal locations of the laser discharge were considered (figure 20) to determine the effect on the surface pressure and heat transfer. A typical result for the surface pressure and heat transfer on the centerline is shown in figure 21. The behavior is similar to the interaction with the sphere alone. Results for different laser focal locations are presented in figure 22 and suggest that an optimal location for the laser discharge may be obtained.

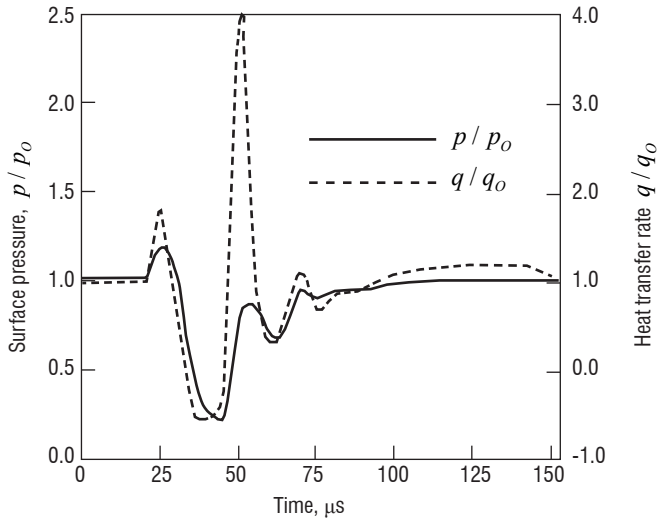

Figure 19 – p/p_O and q/q_O *vs* t for laser discharge [11]

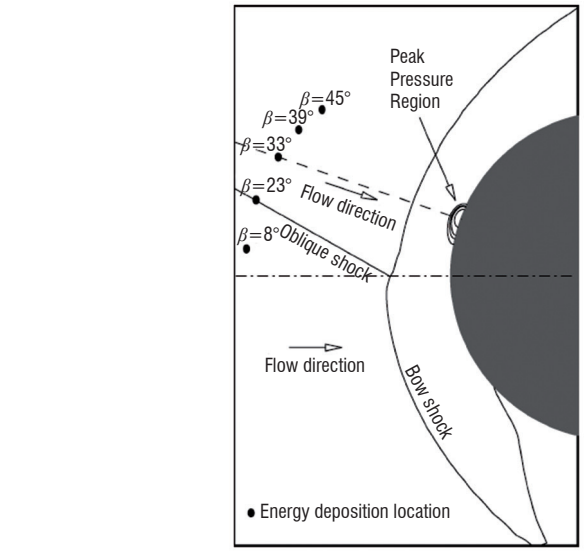

Figure 20 – Laser discharge [11]

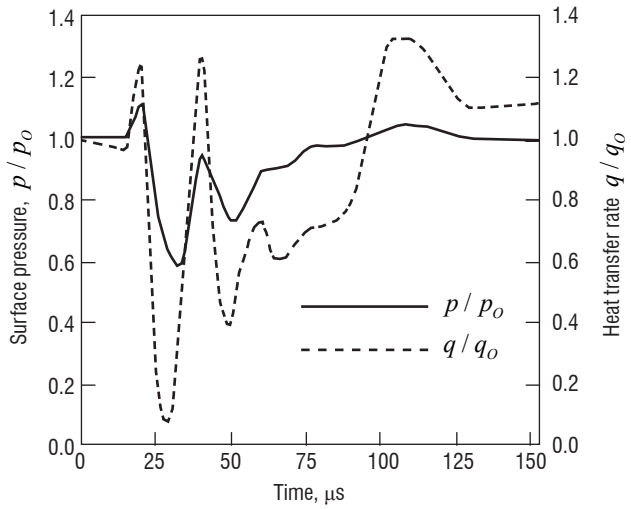

Figure 21 – p/p_O and q/q_O *vs* t for laser discharge [11]

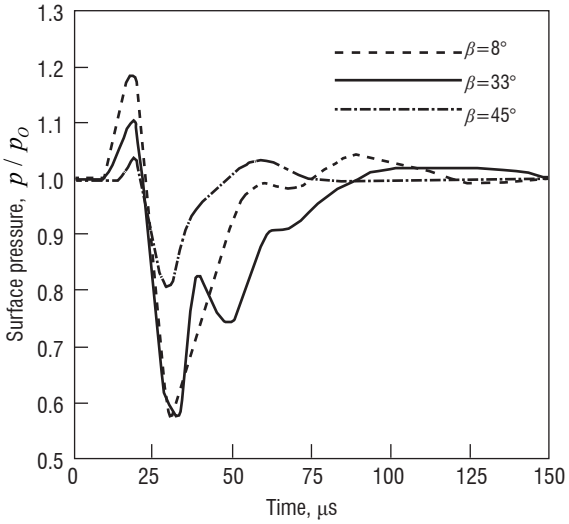

Figure 22 – p/p_O and q/q_O *vs* t for laser discharge [11]

Anderson and Knight

Anderson and Knight [2] simulated the interaction of pulsed heated filaments with a blunt cylinder at Mach 1.89. The flow configuration is shown in figure 23. The flow parameters (table 3) were selected to correspond to the microwave discharge experiments of Kolesnichenko *et al.* [14]. The microwave-generated plasmas were modeled as instantaneously generated filaments defined by density ratio ρ_f/ρ_∞, diameter d/D, length l/D and period L/D where D is the diameter of the cylinder. The simulations were based upon the compressible laminar Navier-Stokes equations for a perfect gas.

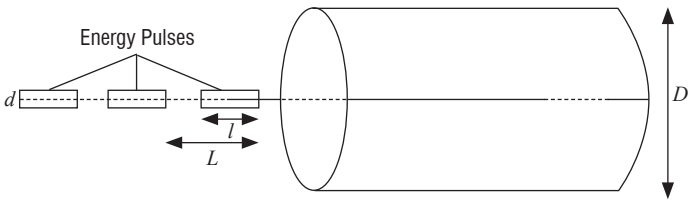

Figure 23 – Flow configuration [2]

Quantity	Symbol	Value
Mach number	M_∞	*1.89*
Reynolds number	Re_D	$7.0.10^4$
Density ratio	α	*0.5*
Filament diameter	*d/D*	*0.1*
Filament length	*l/D*	*1.0*
Filament period	*L/D*	*1.0 to 4*

Table 3 – Flow Parameters

Simulations were performed for four different filament frequencies L/D with a fixed filament length $l/D=1$, diameter $d/D=0.1$ and density ratio α (table 3). Figures 24 to 27 display instantaneous numerical schlieren images (left) and time-averaged streamlines and velocity magnitude contours (right) for four different filament discharge frequencies L/D. The instantaneous images display the lensing upstream of the blunt body shock, formation of a free shear layer due to the interaction of the density interface of the filament with the blunt body shock, and Kelvin-Helmholtz instability. The time-averaged streamlines display the formation of a recirculation region upstream of the cylinder face, and in the particular case $L/D=4/3$ the movement of the stagnation point off the cylinder centerline.

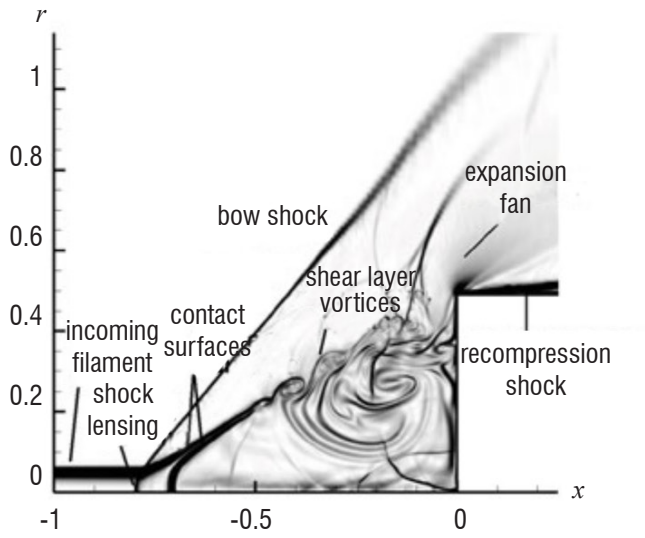

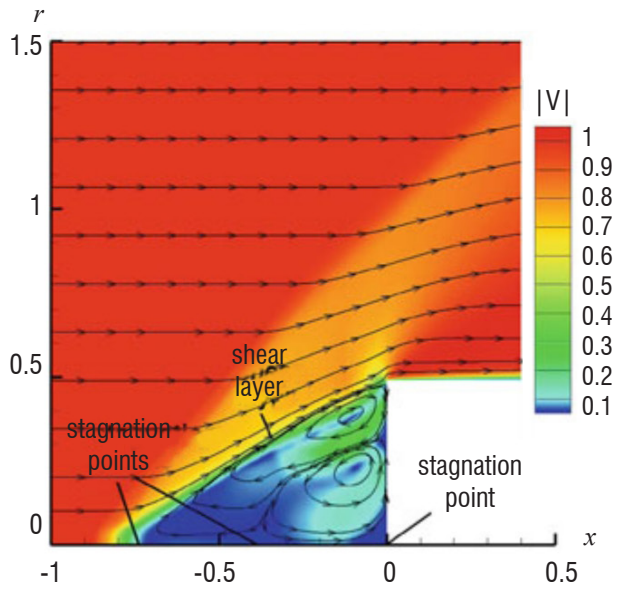

Figure 24 – $L/D=1$ (infinitely long) filament [2]

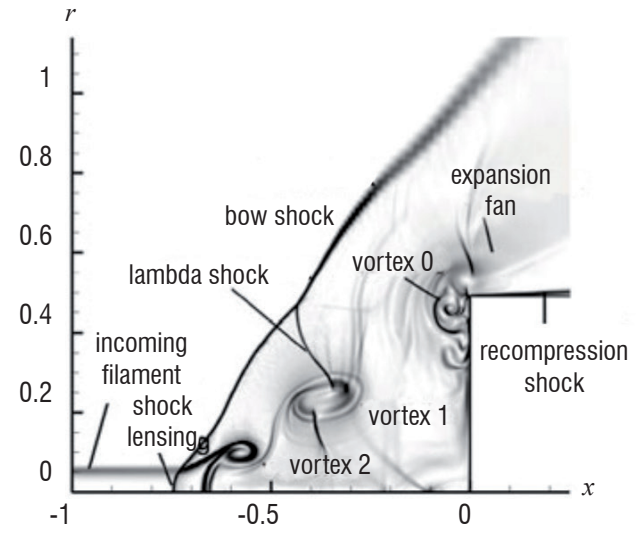

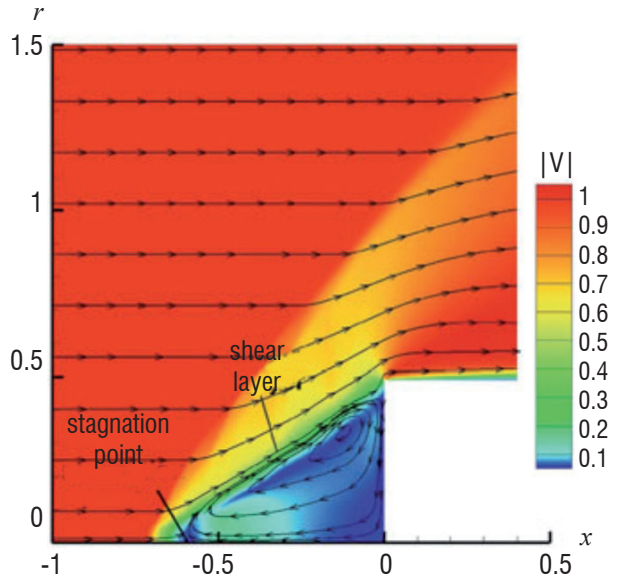

Figure 25 – $L/D=4/3$ filament [2]

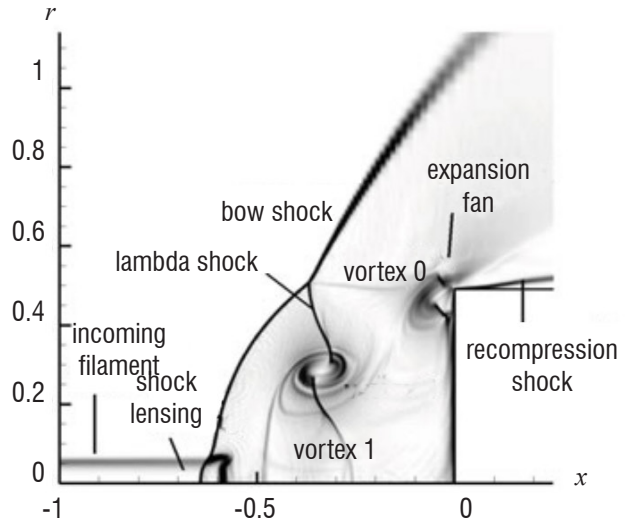

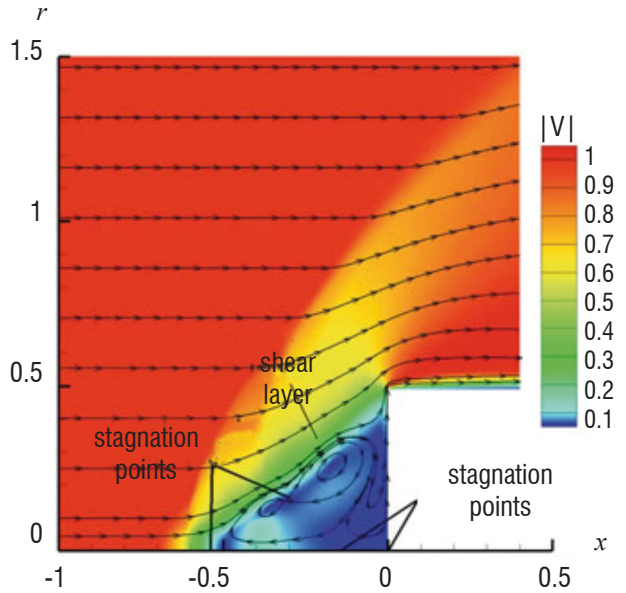

Figure 26 – $L/D=2$ filament [2]

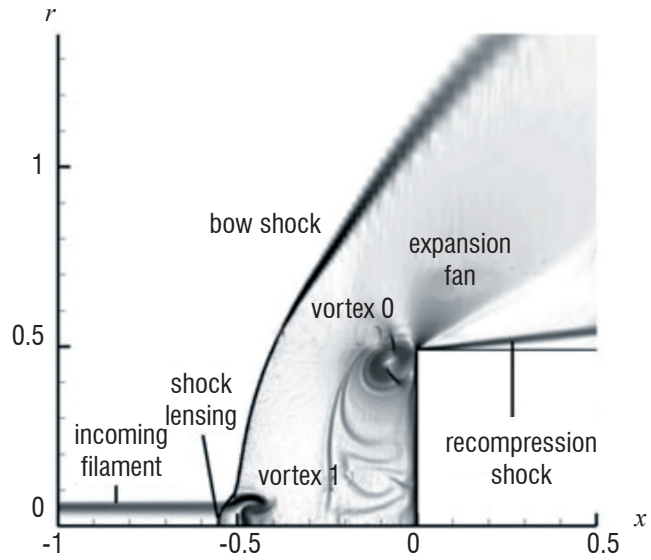

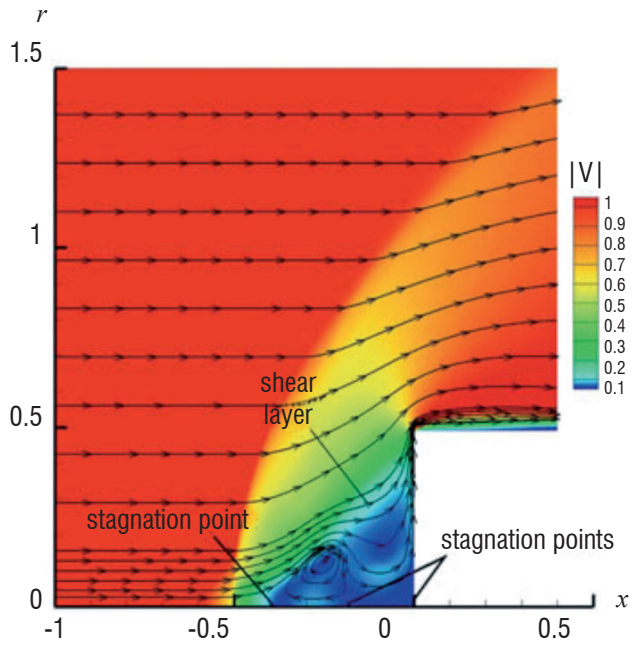

Figure 27 – $L/D=4$ filament [2]

The interaction of the pulsed filaments with the blunt cylinder results in an average reduction in frontal drag at a significant savings in energy. Figure 28 displays the effectiveness ζ defined as the ratio of the average reduction in frontal drag to the baseline (undisturbed flow) drag. Drag reduction up to 40% is observed, with decreasing effectiveness with increasing filament period L/D. Figure 29 shows the efficiency defined as the ratio of the average energy saved due to frontal drag reduction to the energy required to generate the filaments. Efficiencies of a factor of 100 are obtained. Although the filament temperatures are higher than the ambient freestream temperature, there is no detrimental effect on the surface heat transfer to the cylinder face. Figure 30 presents the ratio of the average heat transfer to the cylinder face due to the interaction of the filaments to the undisturbed heat transfer to the cylinder face. Indeed, the average heat transfer is reduced for $L/D=4/3$ due to the movement of the stagnation point off the cylinder face (figure 25).

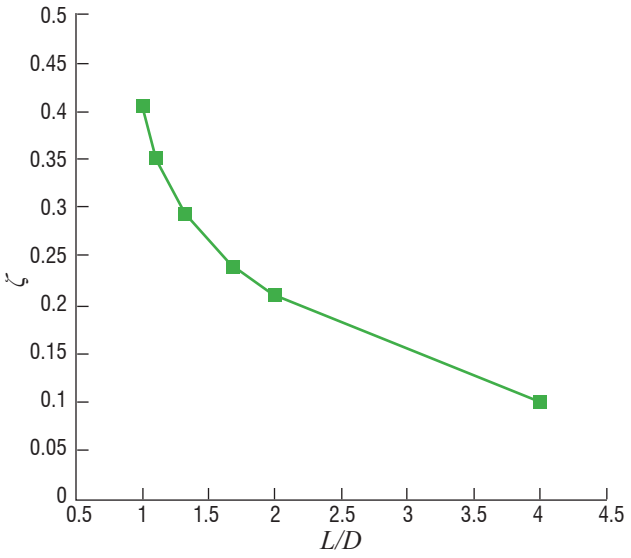

Figure 28 – Effectiveness *vs* L/D [2]

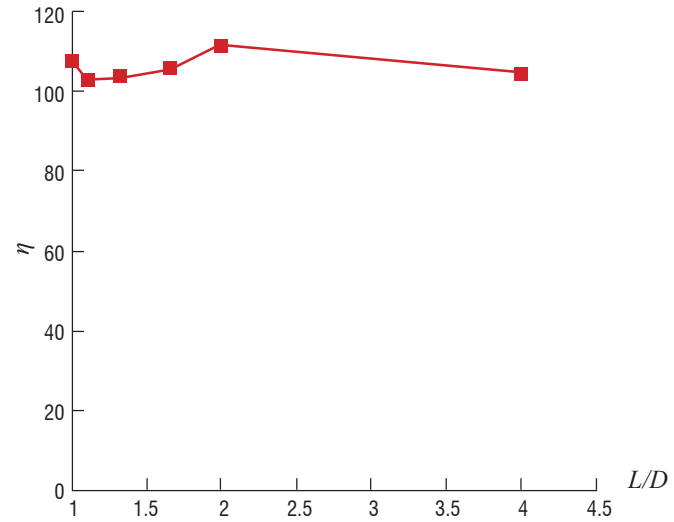

Figure 29 – Efficiency *vs* L/D [2]

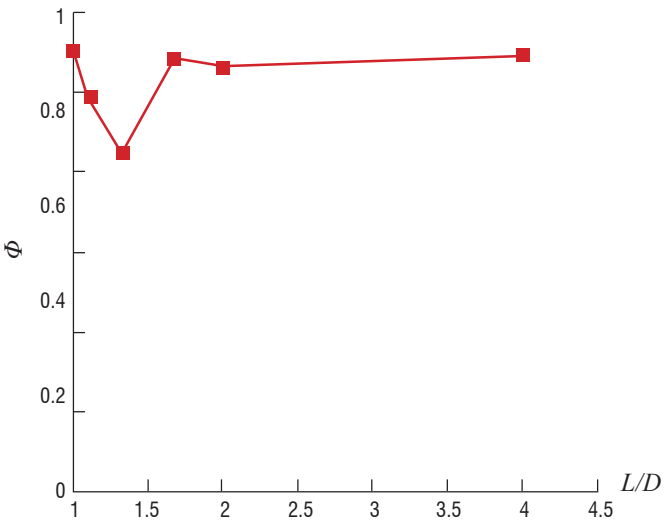

Figure 30 – Heat transfer parameter *vs* L/D [2]

Azarova, Knight and Kolesnichenko

Azarova *et al.* [3] performed a series of simulations of the interaction of an infinitely long heated filament with a blunt cylinder similar to figure 23. The infinitely long filament models repetitive microwave discharges and is characterized by the density ratio ρ_f/ρ_∞ and diameter d/D where D is the cylinder diameter. The flow conditions are indicated in table 4. The computations were based on the compressible Euler equations.

Quantity	Symbol	Value
Mach number	M_∞	*1.89 and 3*
Density ratio	α	*0.4 to 0.6*
Filament diameter	d/D	*0.1, 0.125, 0.25*
Filament length	l/D	∞

Table 4 – Flow Parameters

Contours of density contours at specific times are shown in figure 31 for M_∞=1.89, α=0.5 and d/D=0.25. A Richtmyer-Meshkov instability develops due to the intersection of the heated filament with the blunt body shock (figure 31(a)) forming a single toroidal vortex (V) and lambda shock (P). The bow shock (BS) moves upstream due to the lower Mach number in the filament ($M_f=\sqrt{,\alpha}\ M_\infty$=1.34). As the filament penetrates to the cylinder, a Kelvin-Helmholtz (KH) instability develops due to the slip line (contact discontinuity) generated at the intersection of the boundary of the filament with the blunt body shock. Thereafter a spatially periodic train of vortices forms along the contact discontinuity due to the Kelvin-Helmholtz instability.

A periodic instability forms subsequent to the initial transient. Figure 32(a) shows the location of the blunt body shock on the cylinder axis $X_w(t)$ (note the absolute scale in figure 31(a) and the location of the blunt body shock (BS) on the cylinder axis). The mean shock standoff distance on the centerline due to the filament Δ_f=1.6 Δ where Δ is the shock standoff distance in undisturbed flow. The amplitude of oscillation of the shock standoff distance is approximately 0.16 Δ. The location $X_{T_{max}}$ and magnitude of the maximum static temperature T_{max} are also shown. The periodic behavior of the drag force is also evident (figure 32(b)).

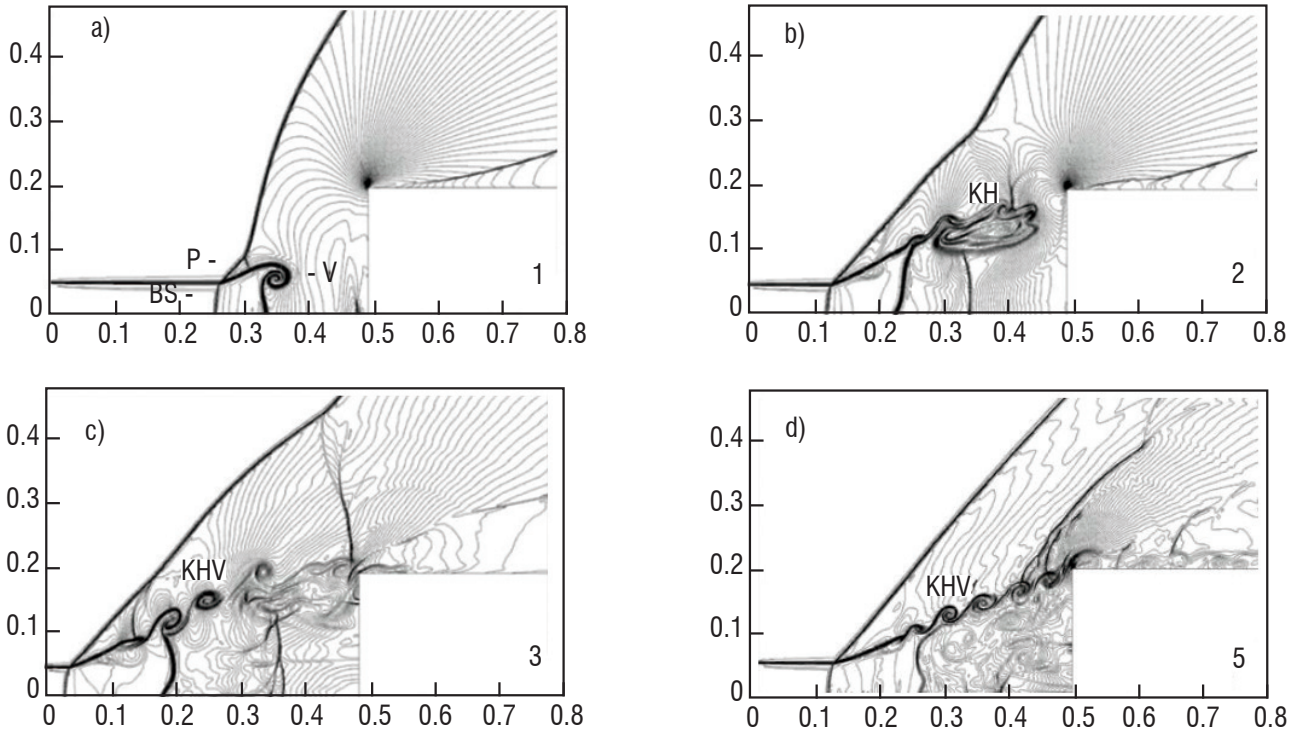

Figure 31 – Density contours for M_∞=1.89, α=0.5, d/D=0.25 [3]

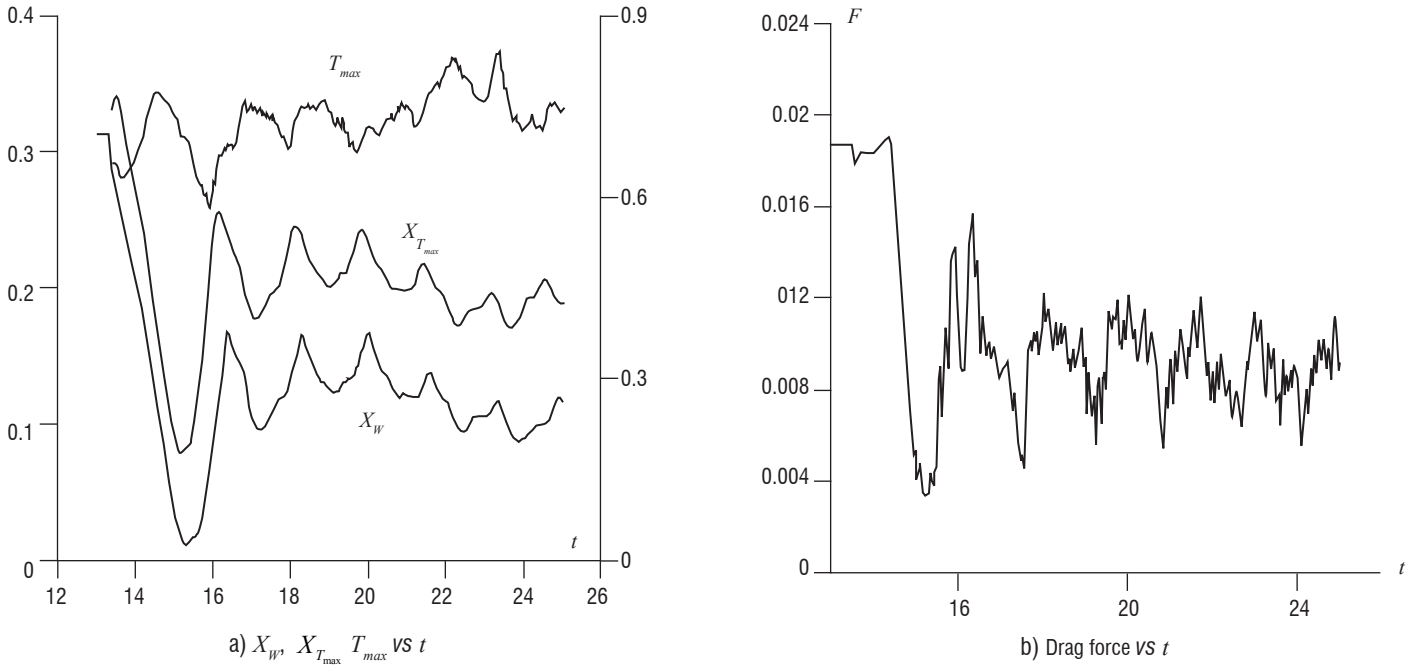

a) X_W, $X_{T_{max}}$ T_{max} *vs* t

b) Drag force *vs* t

Figure 32 – Instabilities at M_∞=1.89, α=0.5, d/D=0.25 [3]

Conclusions

Energy deposition by pulsed laser and microwave discharge is an important area of research for supersonic flow control. Experimental and computational studies have demonstrated the capability for significant reduction in drag on simple geometries. The energy required for the discharge is typically quite small compared to the energy saved through drag reduction.

Future research can focus on applications of pulsed laser and microwave discharge for flight control of supersonic and hypersonic vehicles. The capability to substantially modify the wave structure surrounding a vehicle by energy deposition enables new approaches to flight control. Rather than the conventional method of deforming the vehicle shape (*e.g.*, by means of aileron, elevator, rudder, etc.), the instantaneous pressure distribution on the vehicle can be changed by modifying the wave structure through interaction of pulsed electromagnetic discharges ■

References

[1] R. ADELGREN, H. YAN, G. ELLIOTT, D. KNIGHT, T. BEUTNER and A. ZHELTOVODOV – *Control of Edney IV Interaction by Pulsed Laser Energy Deposition*. AIAA Journal, 43(2):256–269, 2005.

[2] K. ANDERSON and D. KNIGHT – *Interaction of Heated Filaments with a Blunt Cylinder in Supersonic Flow*. Shock Waves, 21:149–161, 2011.

[3] O. AZAROVA, D. KNIGHT and Y. KOLESNICHENKO – *Pulsating Stochastic Flows Accompanying Microwave Filament/Supersonic Shock Layer Interaction*. Shock Waves, 21:439–450, 2011.

[4] E. DAMON and R. TOMLINSON – *Observation of Ionization of Gases by a Ruby Laser*. Applied Optics, 2(5):546–547, May 1963.

[5] B. EDNEY – *Anomalous Heat Transfer and Pressure Distributions on Blunt Bodies at Hypersonic Speeds in the Presence of an Impinging Shock*. FAA Report 115, Aeronautical Research Institute of Sweden, 1968.

[6] R. EXTON, R. BALLA, B. SHIRINZADEH, G. BRAUCHMANN, G. HERRING, J. FUGITT, C. LAZARD and K. KHODATAEV – *On-board Projection of a Microwave Plasma Upstream of a Mach 6 Bow Shock*. Physics of Plasmas, 8(11):5013–5017, 2001.

[7] V. FOMIN, P. TRETYAKOV and J.-P. TARAN – *Flow Control Using Various Plasma and Aerodynamic Approaches (Short Review).* Aerospace Science and Technology, 8:411–421, 2004.

[8] A. FRIDMAN and L. KENNEDY – *Plasma Physics and Engineering.* Taylor & Francis, New York, 2004.

[9] N. GLUMAC, G. ELLIOTT and M. BOGUSZKO – *Temporal and Spatial Evolution of the Thermal Structure of a Laser Spark in Air*. AIAA Journal, 43(9):1984–1993, September 2005.

[10] A. GOLD and B. BEBB. *Theory of Multiphoton Ionization*. Physical Review Letters, 14(3):60–63, 1965.

[11] R. KANDALA and G. CANDLER – *Numerical Studies of Laser-Induced Energy Deposition for Supersonic Flow Control*. AIAA Journal, 42(11):2266–2275, 2004.

[12] D. KNIGHT – *Survey of Aerodynamic Drag Reduction at High Speed by Energy Deposition*. Journal of Propulsion and Power, 24(6):1153–1167, November-December 2008.

[13] Y. KOLESNICHENKO – *Microwave Discharge in Free Space*. Thematic Workshop on Fundamentals of Aerodynamic Flow and Combustion Control by Plasmas, Villa Monastero, Varenna, Italy, EUCASS Aerospace Thematic Workshop (ATW) on Plasmas, May 2007.

[14] Y. KOLESNICHENKO, V. BROVKIN, O. AZAROVA, V. GRUDNITSKY, V. LASHKOV and I. MASHEK – *Microwave Energy Deposition for Aerodynamic Application.* AIAA Paper 2003-0361, American Institute of Aeronautics and Astronautics, January 2003.

[15] Y. KOLESNICHENKO, V. BROVKIN, S. LEONOV, A. KRYLOV, V. LASHKOV, I. MASHEK, A. GORYNYA and M. RYVKIN. *Investigation of AD-Body Interaction with Microwave Discharge Region in Supersonic Flows*. AIAA Paper 2001-0345, American Institute of Aeronautics and Astronautics, January 2001.

[16] I. LASHKOV, I. MASHEK, Y. ANISIMOV, V. IVANOV, Y. KOLESNICHENKO, M. RYVKIN and A. GORYNYA. *Gas Dynamic Effect of Microwave Discharge on Supersonic Cone-Shaped Bodies*. AIAA Paper 2004-0671, American Institute of Aeronautics and Astronautics, January 2004.
[17] Y. LEBEDEV (editor) – *IV International Workshop on Microwave Discharges: Fundamentals and Applications.* United Physical Society of the Russian Federation, Yanus-K., ISBN 5-8037-0066-5,Moscow, 2001.
[18] Y. LEBEDEV (editor) – *VI International Workshop on Microwave Discharges: Fundamentals and Applications.* United Physical Society of the Russian Federation, Yanus-K. ISBN 5-8037-0343-5, Moscow, 2006.
[19] A. MACDONALD. *Microwave Breakdown in Gases.* Wiley Series in Plasma Physics. John Wiley & Sons, New York, NY, 1966.
[20] P. MAKER, R. TERHUNE and C. SAVAGE – *Optical Third Harmonic Generation.* Proceedings of the 3rd International Conference on Quantum Electronics, Columbia University Press, P. GRIVET and N. BLOEMBERGEN (editors), New York, 1963.
[21] R. MEYERAND and A. HAUGHT – *Gas Breakdown at Optical Frequencies.* Physical Review Letters, 11(9):401–403, 1963.
[22] R. MEYERAND and A. HAUGHT – *Optical-Energy Absorption and High-Density Plasma Production.* Physical Review Letters, 13(1):7–9, 1964.
[23] R. MINCK – *Optical Frequency Electrical Discharges in Gases.* Journal of Applied Physics, 35(1):252–254, January 1964.
[24] C. C. MORGAN – *Laser-Induced Breakdown of Gases.* Rep. Prog. Phys., 38:621–665, 1975.
[25] G. OSTROVSKAYA and A. ZAIDEL – *Laser Spark in Gases.* Soviet Physics Uspekhi, 16(6):834–855, 1974.
[26] Y. RAIZER – *Heating of a Gas by a Powerful Light Pulse.* Soviet Physics JETP, 21(5):1009–1017, 1965.
[27] Y. RAIZER – *Breakdown and Heating of Gases Under the Influence of a Laser Beam*. Soviet Physics Uspekhi, 8(5):650–673, 1966.
[28] E. SCHÜLEIN, A. ZHELTOVODOV, E. PIMONOV and M. LOGINOV – *Experimental and Numerical Modeling of the Bow Shock Interaction with Pulse-Heated Air Bubbles*. International Journal of Aerospace Innovations, 2(3):165–187, 2010.
[29] P. TRETYAKOV, A. GARANIN, V. KRAYNEV, A. TUPIKIN and V. YAKOVLEV – I*nvestigation of Local Laser Energy Release Influence on Supersonic Flow by Methods of Aerophysical Experiments*. International Conference on Methods of Aerophysical Research, Novosibirsk, Russia, 1996.
[30] A. ZHELTOVODOV – *Development of the Studies on Energy Deposition for Application to the Problems of Supersonic Aerodynamics*. Preprint 10-2002, Institute of Theoretical and Applied Mechanics, Novosibirsk, Russia, 2002.

Acronym

MW (Microwave)

AUTHOR

Doyle Knight received his PhD in Aeronautics from the California Institute of Technology in 1974. Following two years service in the United States Air Force as an Aeronautical Engineer, and one year Postdoctoral Fellowship in Applied Mathematics at the California Institute of Technology, he joined the faculty of the Department of Mechanical and Aerospace Engineering at Rutgers – The State University of New Jersey. He is Distinguished Professor of Aerospace and Mechanical Engineering. His research interests include gas dynamics and design optimization. His research in gas dynamics includes shock wave boundary layer interaction, incipient separation on pitching airfoils, turbulence model development, high speed inlet unstart and effects of unsteady energy deposition in supersonic flows. His research activity in design optimization focuses on the application of computational fluid dynamics to the automated optimal design of high speed air vehicles.